AIAA JOURNAL
Vol. 43, No. 7, July 2005

Aerodynamic Modification of Supersonic Flow Around Truncated Cone Using Pulsed Electrical Discharges

Daniel Bivolaru* and S. P. Kuo†
Polytechnic University, Brooklyn, New York 11201

An experimental study on the use of plasma to improve blunt body aerodynamics in a supersonic flow is presented. Shadow, schlieren, and plasma glow imaging techniques were used simultaneously for flow and plasma visualization. The discharge current and voltage, as well as the flow pressure and temperature at different locations on the surface of the model, were measured. With a proper aspect ratio 0.81 of the physical spike length to the frontal diameter of a 60-deg truncated cone-cylinder designed for the wind-tunnel model, the on-board pulsed electrical discharge produced a conically distributed plasma around the cathode, which modified the main shock wave structure from a detached bow shock to a tip attached conical shock wave. At discharge maximum, the pressure on the frontal surface of the body decreased by more than 30%, the pressure on the cone surface increased by about 5%, and the pressure on the cylinder surface remained unchanged. The temperature measured near the cone surface increased considerably. The energy consumed in each discharge, which lasted less than 50 ms, was about 150 J. The results demonstrate that a plasma aerospike, conical-shaped plasma distributed around a small slender physical spike, can improve the blunt body aerodynamics.

Nomenclature

D	=	diameter of truncated cone frontal base
D_b	=	diameter of truncated cone base
d	=	diameter of spike/electrode base
L	=	height of truncated cone
l	=	length of spike/electrode
P_0	=	stagnation pressure
p	=	static pressure
T_0	=	stagnation temperature
t	=	time
β	=	angle of shock with respect to horizontal, deg

Subscripts

e	=	on cylinder surface
p	=	perturbed
s	=	on cone surface
t	=	around spike base
u	=	unperturbed
1	=	upstream of shock
2	=	downstream of shock

Introduction

IN a supersonic flow, shock waves introduce additional wave drag to the object, creating a challenge in the design of high-speed vehicles. Therefore, any method to improve the object aerodynamics and reduce this additional wave drag will have a significant positive impact on supersonic and hypersonic vehicles. The obvious gains would be sonic noise attenuation, reduced fuel consumption, and a smaller propulsion system requirement for the same cruise speed. Considerable theoretical and experimental efforts have been devoted to the study of shock waves in supersonic and hypersonic flows. Various approaches to control or modify shock wave structure and position and to develop wave drag-reduction technologies have been explored.

In a theoretical study of interfering flowfields, Busemann (see Refs. 1 and 2) suggested that the geometrical destructive interference of shock waves and expansion waves from two different two-dimensional bodies could work to reduce the wave drag. Ferri[1] and Ferri and Clarke[2] extended this idea to three-dimensional configurations. However, the interference approach is effective only for one Mach number and one angle of attack, which makes the design for practical implementation difficult. A physical spike[3] can be used to improve the body aspect ratio of a blunt body by moving the original bow shock upstream to its tip location in the new form of a conical shock, significantly reducing the associated wave drag. Again, a drawback of a physical spike is its sensitivity to off-design operation of the vehicle, that is, changing the flight Mach number and vehicle angle of attack. A failure regime at aspect ratios less than one also prohibits the practical use of a physical spike alone for shock wave modification.

A variety of ideas, based on using electromagnetic forces to affect the lift and drag of flying bodies, have been proposed to minimize the negative effect of shock wave formation on flight by indirect boundary-layer flow control. However, an ionized component in the flow has to be generated so that the fluid motion can be controlled, for instance by a $\boldsymbol{j} \times \boldsymbol{B}$ force density, where $\boldsymbol{j}$ and $\boldsymbol{B}$ are the applied current density and magnetic field in the flow, respectively. The current driven by the induced $\boldsymbol{V} \times \boldsymbol{B}$ field in the moving plasma fluid, where $\boldsymbol{V}$ is the velocity of the plasma fluid, can also cause changes in the properties and stability of the gas flow due to ohmic heating.[4–6] A similar effect can be introduced to the flow by applying an electric field to induce paraelectric and peristaltic electrohydrodynamic effects.[7] For practical aerospace applications, the applied electrostatic voltage can be significantly larger than the induced electromotive force, by orders of magnitude.[7] However, the study of electroaerodynamic applications is mainly focused on subsonic speed boundary-layer flow control for drag increase or reduction,[7] or for lift and thrust.[8]

Energy deposition in front of the flying body to perturb the incoming flow and shock wave formation has been studied extensively. In a paper investigating hypersonic flow around blunt bodies, Katzen and Kaattari[9] outlined briefly the predicted aerodynamic effects arising from gas injection in the subsonic region of the shock layer. In one particular case, when helium was injected at supersonic speed, the flow penetrated the bow shock, creating an irregular shock wave of conical shape with the vertex at a distance of about one body

Received 31 December 2003; revision received 21 October 2004; accepted for publication 1 December 2004.

*Research Scientist, Department of Electrical and Computer Engineering, 6 Metrotech Center; dbivola@duke.poly.edu. Member AIAA.

†Professor, Department of Electrical and Computer Engineering, 6 Metrotech Center. Member AIAA.

diameter from the body. Gordeev et al.[10] carried out an experiment injecting a high-pressure plasma from a cone–cylinder model into an upcoming supersonic flow. The plasma, generated in a chamber inside the model with a high current electrical discharge initiated by an exploding wire, was injected forward into the flow through a convergent–divergent nozzle placed axially inside the model. Significant drag reduction was reported. Laser beams were used to deposit energy into the flow by multiphoton gas ionization, subsequent plasma absorption of laser radiation, and gas heating. In experiments of directed laser energy in hypersonic flow,[11,12] a smaller plasma region was obtained at the focal point of the laser beam in front of the body. The high-temperature region considerably modified the initial plasma structure distributed on the body surface (generated by the high-enthalpy flow itself). A focused microwave beam was also used to deposit energy in front of an object. A lens placed in front of a microwave horn antenna (Ku band) was used for focusing, and a beta radiation source (^{90}Sr) was used for seeding the microwave plasma, which was generated in multilayers ahead of the bow shock in a Mach 6 flow.[13] Although the main discharge localized in the bow shock region, the microwave power used in the experiment was too low to achieve noticeable plasma effects on the flow structure.

Levin and Tarenteva[14] and Riggins et al.[15] carried out numerical simulations on the utilization of focused thermal energy for flow modification around blunt bodies in high-speed flows using ideal models. The results showed that the thermal energy deposition in front of the object could have a positive effect on the shock structure. When sufficient energy was provided, a weak shock was formed around the energized region, and the blunt-body main shock was weakened and moved upstream. Consequently, depending on the amount of energy injected, rapid lateral transitions of this shock into an oblique shock is seen to couple with the shock at the energized region and to envelop the frontal surface of the body (without forming any secondary shocks). This is similar to that observed in the experiments using focused laser beams.

Plasma for flow modification can be generated by onboard electrical discharges of different geometries. The difficulty of this method is to control the location of the discharge. Recent experiments[16,17] used an arc discharge (60 Hz) to generate pulsed plasma around the tip of a cone-shaped model. The shadow imaging visualization of the flowfield (at a 30-Hz frame rate) showed that the plasma interacted with the flow and moved the shock wave front upstream of the model. Although the time evolution of this unsteady forward-moving shock wave could not be recorded in real time due to the low-speed camera used for flow visualization, significant shock wave structure and standoff change by the discharge were observed. The power used in the experiment was significantly lower than those used in numerical simulations studying the thermal energy deposition effect.[14,15]

In the present work, the results of an experimental study on the aerodynamic influence of on-board generated plasma by pulsed electrical discharges in the frontal region of a blunt body are reported. A truncated cone model with an attached physical spike, immersed in Mach 2.5 airflow, is used as shock wave and plasma generator.[18,19] The flow and plasma are investigated by means of shadow and schlieren imaging techniques, temperature and pressure probes placed on the model surface, plasma glow visualization, and discharge current and voltage measurements.

Experiment

Experimental Conditions

The experiments were carried out in a supersonic blowdown wind tunnel exhausting to the atmosphere. This facility has a test section of 0.38×0.38 m cross section. The pressure and temperature of the steady-state Mach 2.5 flow are 0.2×10^5 N/m^2 and 135 K, respectively. Physical and optical access to the test section is via two transparent round windows of 0.38 m in diameter, one on each side of the test section. A detailed description of the facility can be found in Ref. 19.

A wind-tunnel model was used as shock wave and plasma generator. A photograph of the model is shown in Fig. 1a. The model consists of a truncated 60-deg cone having a height of $L = 12.7$ mm

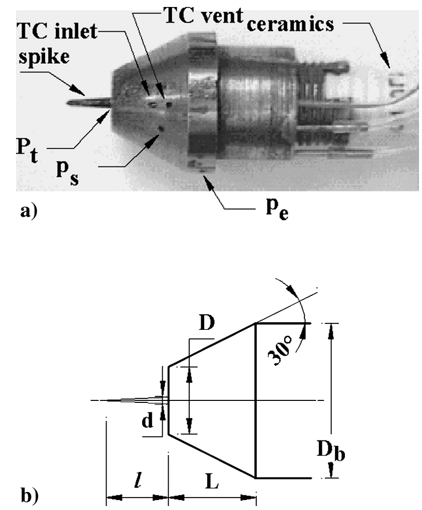

Fig. 1 Model: a) side view, instrumented with pressure taps and built-in thermocouple probe and b) schematic of truncated cone/spike to indicate dimensions.

and a ceramic-insulated central electrode protruding axially outward. The diameters of the truncated cone bases are $D_b = 25.4$ mm and $D = 11.1$ mm, respectively. These dimensions are indicated in Fig. 1b. The conical model is attached to a cylinder with a length of 120 mm and a diameter D_b. The discharge gap between the central electrode and the inner surface of the cone is 3.75 mm. The slender part of the central electrode was finely machined to different shapes: pinpointed conoidal, conoid with a parabolic tip, paraboloidal, or hyperboloidal. The length l of the protruding part of the central spike/electrode varied from 3 to 16.5 mm, but had a constant diameter of 1.5 mm. The aspect ratio of spike length to model frontal diameter l/D varied from 0.27 to 1.49.

The wind-tunnel model is instrumented with pressure taps on the cone surface p_s and cylinder surface p_e, as well as axially on the model frontal surface by introducing a clearance between the inner surface of the ceramic and the outer surface of the spike/cathode P_t. The static pressure taps were made by drilling holes on the cone and cylinder surfaces at $x = 19.2$ and 27.5 mm, respectively, where x is the axial coordinate of the model with $x = 0$ set at the spike tip. These taps were connected through adequate tubing to high-speed piezoelectric transducers (83-μs response time) located outside of the wind tunnel.

The gas temperature measurements were performed at $x = 18$ mm on the surface of the model by using an ungrounded 0.5-mm-diam thermocouple (TC). The probe was placed in a ventilated cavity (1-mm diameter and 2 mm long) made by drilling into the model parallel to its axis. The cavity had a vent area to entrance area ratio of about 1:4. This geometry provided a lower heat loss by radiation, a better than 0.45-s response time, and good electrical shielding against the noisy plasma environment.

In addition to the model instrumentation, in the topside region of the model, a pitot probe was used to monitor selectively the total pressure of the flow in front of, or behind, the oblique portion of the main shock wave structure generated by the model.

Experimental Arrangement

A schematic of the experimental arrangement is shown in Fig. 2. The base of the model is connected to the wind tunnel that is electrically grounded (GND), and the central electrode can be selectively connected to a positive or negative voltage (HV). A variable 0–6 kV at 400-mA dc power supply applies a constant voltage (V) to a low-duty cycle self-oscillating circuit, which consists of a charging resistor R, an energy storage capacitor C, and the plasma device load. The series resistor R_p limits the discharge current at about 10–40 A. The circuit components were adjusted during the experiments to achieve optimal conditions for discharge energy, pulse length, and repetition rate. The values used to obtain the results reported in the present work are $R = 20$ kΩ, $C = 148$ μF,

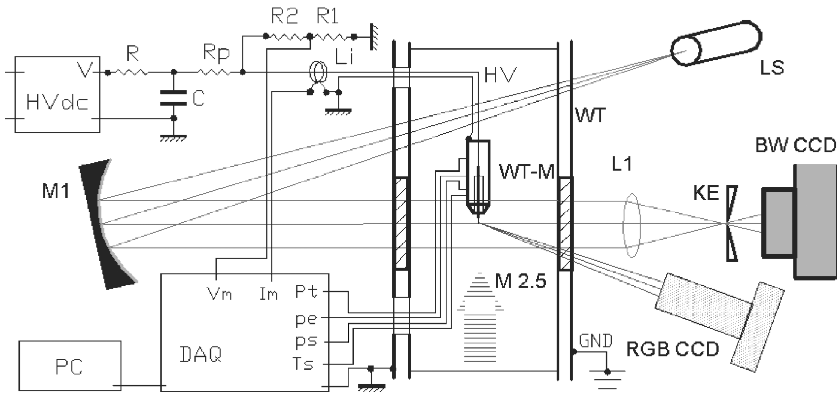

Fig. 2 Schematic of experiment.

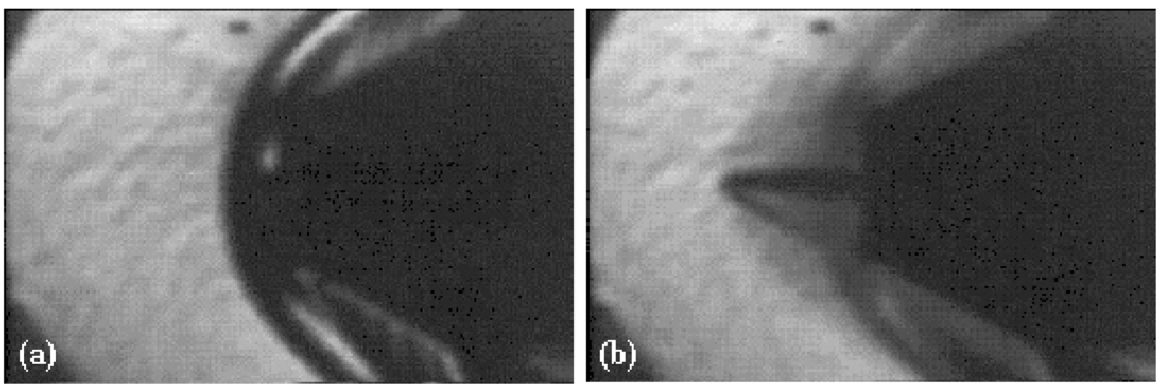

Fig. 3 Schlieren images of a Mach 2.5 flow over 60-deg truncated cone with attached slender physical spike: a) *l/D* = 0.27 and b) *l/D* = 0.81.

and $R_p = 75\ \Omega$. During the wind-tunnel run, each discharge lasted less than 50 ms and its repetition time varied from 1.13 to 1.32 s, depending on the voltage applied, electrode geometry, and flow conditions.

A current loop (Li) with 0.1 V/A calibration was adopted to measure the plasma discharge current, despite that it could give some errors due to its nonuniform frequency response in the low-frequency region. A voltage divider with a ratio $R_1/(R_1 + R_2)$ of 1:500, together with a 1:10 voltage probe, was used for the voltage measurements. A multichannel data acquisition system (DAQ + personal computer) recorded the signals from the voltage V_m and current I_m probes and from the wind-tunnel and model pressure (P_{01}, P_t, p_e, and p_s) and the temperature (T_{01}, T_{0s}) sensors.

The visualization of the flowfield was obtained through shadow, schlieren, and plasma luminosity video imaging. An incandescent lamp (LS) with beam-forming optics and filters was used as a light source for the combined shadow/schlieren system. A parabolic mirror (M1), having a diameter of 0.3 m and focal length of 3.7 m, collimated the divergent beam from the light source through the wind-tunnel test section windows. On the other side of the wind tunnel, an image-forming optical system, consisting of a lens (L1), a light ray selecting device (KE), and a black and white (BW) high-resolution charge-coupled device (CCD) camera was used to obtain the shadow and schlieren images. The beam-selecting device used in the schlieren imaging technique was a knife edge with different configurations, including pinholes and horizontal or vertical narrow slits. No beam-selecting device was needed for shadow imaging. The light beam was projected directly on the CCD area and recorded at a rate of 30 frames/s with an exposure time of 1/60 s. In the case of shadow imaging, the image plane of the system was moved much farther away from the light source, to reduce the unwanted background light coming from the discharge, but with a compromise between image quality and contrast.

A color CCD camera (RGB) was used for plasma luminosity recording. The camera was positioned on either side of the wind tunnel at a small angle to the optical axis of the shadow/schlieren imaging system. This video camera recorded at a rate of 30 frames/s with selectable exposure time from 1/60 to 1/4000 s. A neutral density filter was used to reduce the airglow intensity of the discharge entering the camera. The synchronization between the shadow/schlieren and the plasma luminosity recordings was realized by postprocessing of the corresponding images (extracted frames) that contained the discharge glow. Tracking of video frames showed that the frame synchronization error between cameras during one-run duration (100–300 frames) was less than one-half frame, that is, less than 1/60 s.

Results

Supersonic Flow Properties in Absence of Plasma

Two schlieren images of the Mach 2.5 flow over the 60-deg angle truncated cone model with an attached paraboloidal physical spike are shown in Fig. 3. In Fig. 3a, the aspect ratio of the spike length to the spike diameter l/d is two, and it is six in Fig. 3b. The flow direction is from left to right. The aspect ratios l/D in Figs. 3a and 3b are 0.27 and 0.81, corresponding to spike lengths of 3 and 9 mm. The images were taken using a pinhole knife edge of 0.2 mm in diameter. The shading differences in the schlieren images reflect the density variation in a plane perpendicular to the optical axis, which is perpendicular to the flow. The exposure time of the images is 1/4000 s. The pressure and temperature of the steady-state flow are 0.2×10^5 N/m^2 and 135 K.

As shown in Fig. 3a the spike with a very small aspect ratio has practically no effect on the detached curved shock in front of the model. The increase of the spike length leads to noticeable perturbation to the flow upstream of the curved shock by modifying the shock structure in that region to a conical shock structure attached to the spike tip, as shown in Fig. 3b. For large l/D, the flow is expected to become conical, with the vertex starting near the boundary separation region around the spike tip.[3] This is indeed the case because the spike length increases to $l/D = 1.49$ (not shown in Fig. 3). Only a conical shock structure attached to the spike tip is observed; the boundary layer separates from the spike surface with the separation point located at the tip of the spike and the reattachment points near the body shoulder.

Supersonic Flow Interaction with Plasma

In previous experiments,[16] both negative and positive voltages were applied to the central electrode (with respect to the body of the model connected to the ground). Despite having similar discharge energies in both cases, in the case of using the central electrode as the anode, the produced plasma could not extend to the front region of the shock wave and, thus, did not visibly influence the shock structure. Therefore, in all cases presented in the following text, the spike was used as the cathode.

Consider first the case with $l/D = 0.81$. The wind-tunnel model with this arrangement generates a shock wave structure shown in Fig. 3b. The slender physical spike only slightly modifies the curved shock wave structure in the central region around the spike, where the shock front becomes conical attached to the spike tip.

The time evolution of the plasma pulse is shown in Fig. 4. Two consecutive frames of plasma luminosity (Figs. 4a and 4b) and the corresponding schlieren images of the flowfield (Figs. 4c and 4d) were extracted from video recordings. The time between two consecutive frames is 1/30 s with an exposure time of 1/60 s for schlieren and 1/4000 s for plasma glow images. The wind-tunnel model can also be seen as an object in Figs. 4a and 4b and as a shadow in Figs. 4c and 4d. The schlieren imaging of the flow is obtained by using the optical setup having a pinhole knife edge of 0.2 mm in diameter.

The discharge started at the cathode base and expanded upstream along the cathode surface in less than 1/30 s (one frame). The shape of the discharge evolved from initial discoid shape at the base (Fig. 4a) to a conical shape around the cathode as shown in Fig. 4b. Note that the plasma shown in Fig. 4a is located behind the curved shock front shown in the corresponding schlieren image (Fig. 4c). The flow pattern of Fig. 4c is found to be almost identical to that shown in Fig. 3b, indicating that there is a negligible plasma effect on the shock wave.

On the other hand, fully expanded plasma glow distributing in the frontal region of the original curved shock front and appearing in the shape of a conical sheath around the cathode is observed in Fig. 4c. The corresponding schlieren image shown in Fig. 4d becomes quite different from that shown in Fig. 3b, evidencing significant modification on the shock wave structure. The plasma distribution, as indicated by its glow image, has a conical shape with an almost similar angle to that of the truncated part of the model (60 deg), which is smaller than the angle of the newly formed oblique shock front appearing in Fig. 4d. The new shock wave structure resembles the shock front of a conical shock attached to the tip of the spike, which is radically different from the original shock structure shown in Fig. 3b, which is dominated by a curved shock structure. Moreover, in the central region, the angle of this new conical shock is slightly larger than the angle of the original shock front.

A set of frames similar to those in Figs. 4b and 4d to demonstrate the significant plasma effect on the shock wave structure has been presented in an earlier paper.[18] Here, Figs. 4b and 4d are included for a comparison with the corresponding images in Figs. 4a and 4c, to single out an observation; namely, a significant plasma effect on the shock wave was observed only when the plasma was generated in a conical shape in the region upstream of the modified shock structure (in this case, the curved shock).

We now return to the case of Fig. 3a to show the importance of the spike aspect ratio l/D to the plasma influence on the shock wave structure. In the absence of plasma, the spike/cathode with length of 3 mm or $l/D = 0.27$ has negligible influence on the flow, and a curved shock structure is observed. In Fig. 5a, the discharge luminosity in the schlieren image shows clearly that the plasma was generated behind this curved shock.

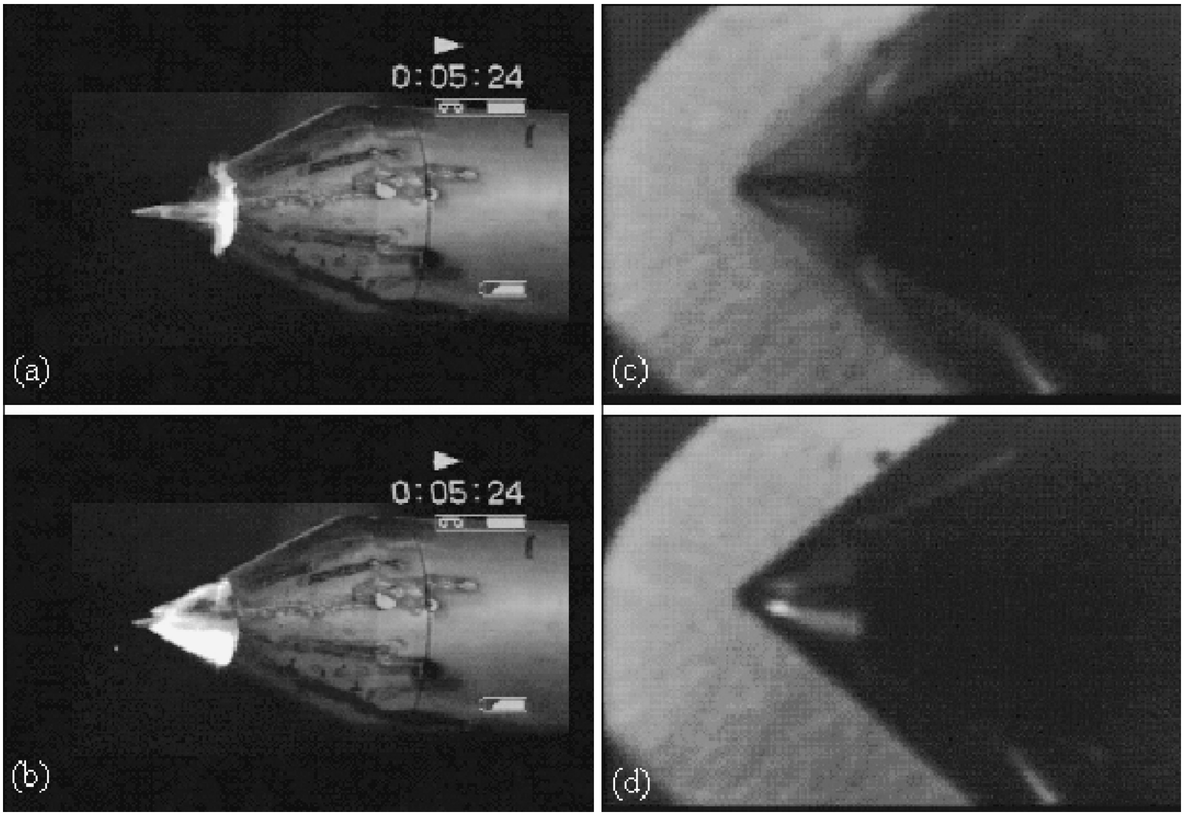

Fig. 4 Images a) and b) time sequence of plasma discharge luminosity in 1/30-s time step and c) and d) corresponding schlieren images; traces on model surface in frames a and b are randomly moving anode spots of discharge in stagnant air.

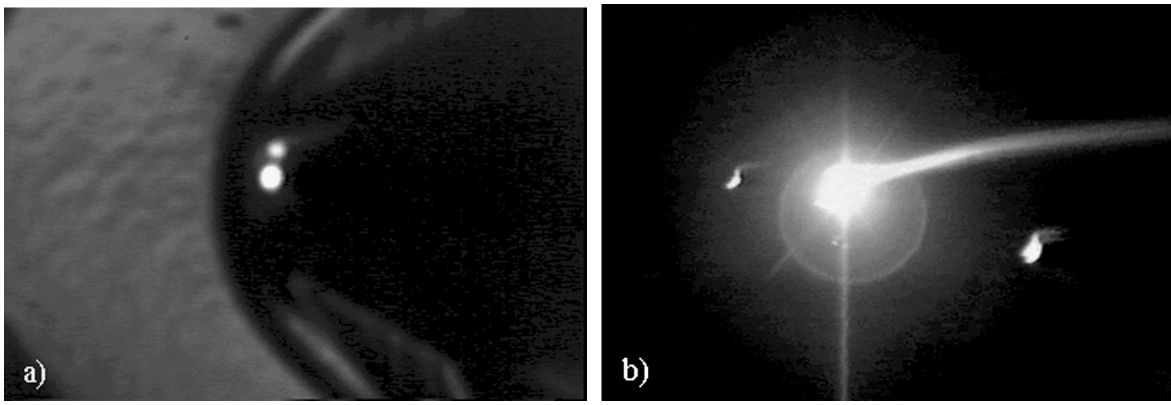

Fig. 5 Images: a) schlieren photograph of flow during an onboard electrical discharge and b) corresponding plasma glow image; cathode-spike aspect ratio is $l/D = 0.27$.

The average discharge power is about the same as that applied in the preceding case using a much longer spike with $l/D = 0.81$. However, no noticeable plasma effect on the shock wave structure can be found when comparing it with that in the unperturbed flow (Fig. 3a). In fact, the local heating by the discharge in the case of the shorter spike is much greater than that of the longer spike. This is confirmed by the corresponding glow image (Fig. 5b), which shows a stronger light intensity emitted from a more localized region as compared with the airglow intensity and distribution captured in Fig. 4b. This comparison suggests that the thermal effect on the shock structure may be small in these experiments. It also reveals the importance of the plasma location. Only when plasma is localized upstream (or ahead) of the curved shock generated by the blunt body (Fig. 4b) is significant modification of the shock structure achieved (Fig. 4d).

The changes of the main shock front and the local shock angle due to the plasma pulse are qualitatively represented in Fig. 6. A digital edge detection technique was applied to the schlieren images (Figs. 3b and 4d) of the flow before and during the plasma pulse, as well as the image of the model in the absence of the flow. The results were then superimposed in Fig. 6a. The bow shock front of the blunt body, that is, the truncated cone, in Fig. 3b and the oblique shock front in Fig. 4d appear in Fig. 6a as a curved line and a straight line at an angle of about 41-deg, respectively. The spike shock front attached to the tip in Fig. 3b was not detected, and, thus, its representation is missing in Fig. 6a. The average local shock wave angles in both cases are plotted against the axial coordinate x of the model. The results are presented in Fig. 6b. The spike, cone, and cylinder projection angle measured from the model axis are shown as straight lines. The relatively high fluctuations in the shock wave angles, in both cases, are attributed to the inaccuracy of the edge detection and local angle calculations techniques. Note that the curved shock angle and the oblique shock angle approach to the same angle at an axial distance away from the tip of the spike greater than one body diameter.

The results presented in Fig. 6a indicate that, during the plasma pulse, the spike shock and the bow shock of the blunt body unify into a single conical shock attached to the tip of the spike.

In the frontal region ($x < 9$ mm) of the model, the conical shock front is located farther away from the frontal surface of the truncated cone than the shock fronts of the spike and the blunt body. It is reversed in the conical surface region (9 mm $< x <$ 22 mm) of the truncated cone. Therefore, one would expect a pressure drop on the frontal surface and a pressure increase on the conical surface during the plasma pulse, as will be shown by the pressure measurement to indeed be the case.

Discharge Power and Energy

The voltage–current product represents the instantaneous power P of the discharge during a wind-tunnel run (about 5.3-s supersonic

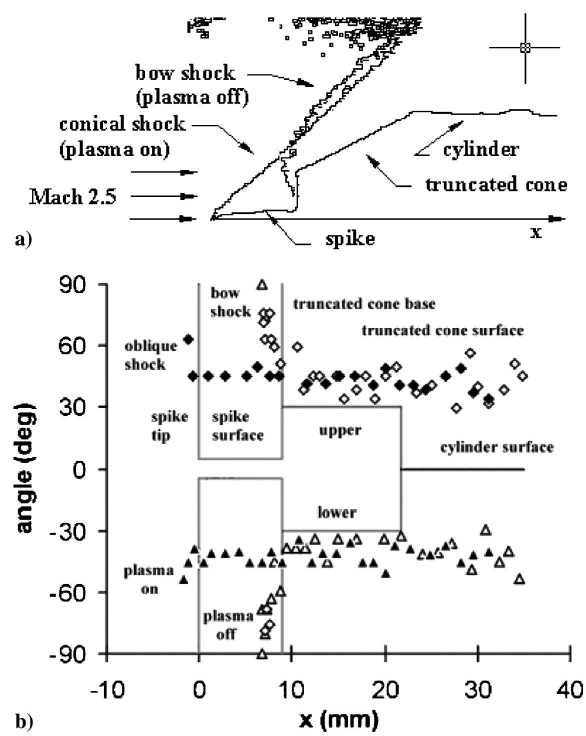

Fig. 6 Main shock wave location and angle: a) shock front location before and during plasma pulse determined by edge detection technique and b) corresponding shock wave angle vs axial coordinate x of model with $x = 0$ at cathode tip.

flow) and is presented in Fig. 7. The power function of the discharge during supersonic flow, at $t = 3.9$ s, is shown in greater detail in the upper right-hand corner of Fig. 7. The first part of the power function, a large peak, is attributed to the main discharge lasting about 10 ms. Shortly after gas breakdown occurs, the discharge current increases rapidly in less than 1 ms to a very large value of about 20 A. Consequently, the discharge sustaining voltage decreases rapidly from 3.2 kV to a very low level of about 200 V.

The peak power of this pulse is about 45 kW. The second part of the power function has a slow decay and a pulse length of ~30 ms, function of the flow condition. The total energy in this discharge pulse is about 150 J. Note that this peak power is 4.5 times smaller than that of the discharge recorded at $t = 1.45$ s when the flow speed is subsonic.

Surface Pressure

The result of the static pressure measurement by a tap placed on the truncated cone surface at a distance $x = 19.2$ mm from the tip

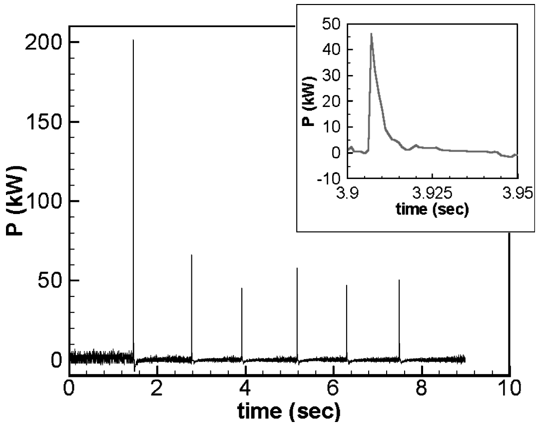

Fig. 7 Power of self-triggered electrical discharges during wind-tunnel run; airflow is supersonic (Mach 2.5) in time interval from $t = 2.3$ to 7.6 s.

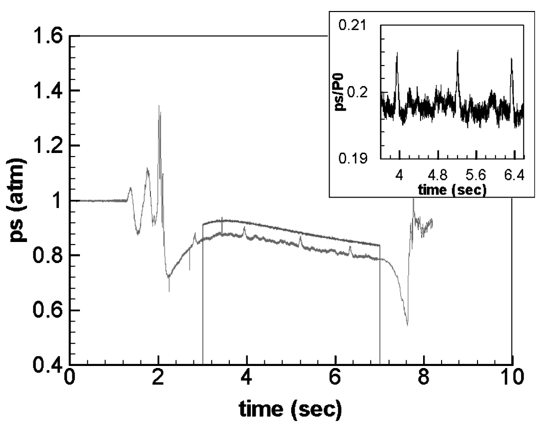

Fig. 8 Pressure measurement by tap placed on truncated cone surface at $x = 19.2$ mm from tip compared to numerical result for an ideal Mach 2.5 supersonic conical flow with shock wave angle of $\beta = 41$ deg.

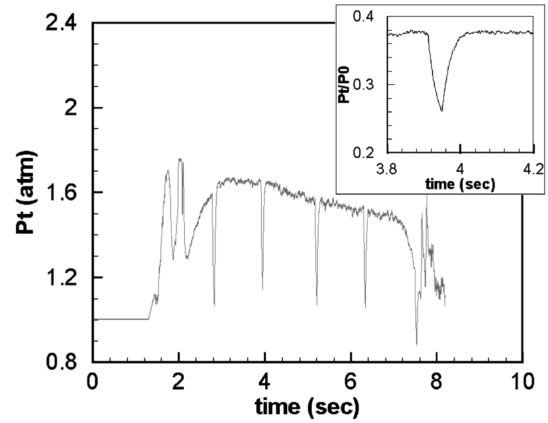

Fig. 9 Pressure P_t measured by axial tap located on frontal surface of model; downward pressure spikes are induced by electrical discharges.

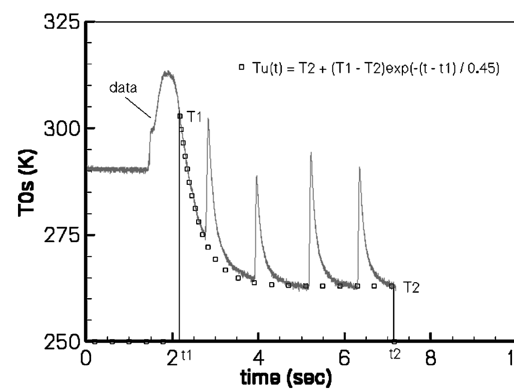

Fig. 10 Temperature curve fit (□) on temperature profile of perturbed supersonic flow after transition from subsonic to supersonic; sections representing unperturbed temperature are matched closely by exponential decay function with time constant of 0.45 s.

is shown in Fig. 8. The normalized pressure p_s/P_{01} by the stagnation chamber pressure P_{01} is shown in the upper right-hand corner of Fig. 8. In the experimental data shown in Fig. 8, the four positive pressure spikes located between $t = 2.5$ and 7 s represent the pressure perturbed by the plasma, showing about a 4% increase (3.99×103 N/m$^2|_{t=3.9\ \mathrm{s}}$) from the unperturbed one.

On the other hand, the numerically calculated pressure, based on the Taylor–Maccoll approximation for an ideal Mach 2.5 conical flow and an attached oblique shock wave with an angle of $\beta = 41$ deg, is also about 5% higher than the pressure in the case of curved shock. The close agreement between the results of measurement and calculation suggests that the flow during the plasma pulse behaves similarly to a conical flow.

Figure 9 shows the pressure P_t and the normalized pressure P_t/P_{01}, measured by the axial tap placed on the frontal surface of the model around the tip base. In the absence of plasma, the average normalized unperturbed pressure measured by the axial tap is about $P_t/P_{01} = 0.37$. (The normalized total pressure measured in the wind-tunnel test section using a pitot probe is on the average of $P_{02}/P_{01} = 0.47$.) The four negative pressure peaks located between $t = 2.5$ and 7 s during supersonic flow represent the pressure decrease caused by the pulsed plasma. The maximum pressure decrease, of about 50.7×10^3 N/m^2, in each discharge is more than 30% of the unperturbed pressure.

The pressure measured on the cylinder surface behind the expansion fan region p_e did not show any noticeable changes from the unperturbed pressure. The average normalized pressure during the same time interval, between $t = 2.5$ and 7 s of the wind-tunnel run, is $p_e/P_{01} = 0.051$.

Surface Temperature and Heat Pulse Reconstruction

The response time of the thermocouple system is too long to measure directly the flow temperature on the surface of the model during the discharge pulse. Hence, an overall energy balance on the thermocouple system is used to calculate the actual gas temperature from the measured temperature. When radiation loss and temperature gradient are neglected in the probe, the gas temperature on the cone surface T_{0p} is related to the measured total temperature function $T_{0s}(t)$ by the equation $T_{0p}(t) = \tau T'_{0s}(t) + T_{0s}(t)$, where $\tau = m_s c_s / h A_s$ is the thermocouple system time constant and the prime stands for time derivative. The thermocouple mass m_s, specific heat c_s, and area A_s have known values, but the convection heat transfer coefficient h between the thermocouple and fluid is difficult to determine for a specific geometry and gas composition. Thus, this response time constant needs to be measured experimentally.

The unperturbed temperature measurement presented in Fig. 10, together with the plasma-induced temperature perturbation, shows that it takes additional time for the temperature system to reach the gas steady-state temperature.

Hence, we estimated the time constant by measuring the time needed for the temperature system to reach $(1 - 1/e)$ of the steady-state temperature value after the step decrease in temperature on the cone surface during the transition from subsonic to supersonic flow. A function fit of the unperturbed temperature T_{0u} decay (sampled during the steady-state flow in the absence of plasma) is shown in Fig. 10. The exponential function $T_{0u}(t) = T_2 + (T_1 - T_2)\exp[-(t - t_1)/\tau]$ with a time constant $\tau = 0.45$ s is the best fit to the measurement, where $T_1 = T_{0s}(t_1)$ and $T_2 = T_{0s}(t_2)$ are the temperature values measured at the limits of the selected time interval $[t_1 t_2]$ when the flow is supersonic. Therefore, the thermocouple time constant is $\tau = 0.45$ s.

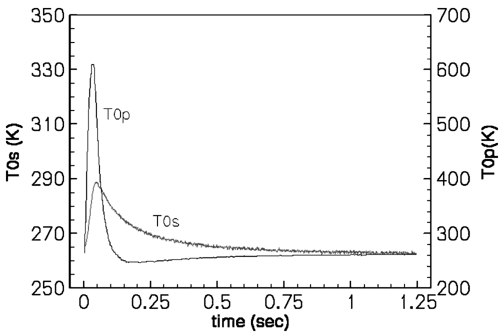

Fig. 11 Measured T_{0s} and predicted temperature pulse T_{0p} on cone surface at $t = 4$ s of wind tunnel run; temperature probe time constant of $\tau = 0.45$ s used for calculations.

The reconstructed temperature function on the surface of the cone at $t = 3.9$ s, using the time constant calculated earlier, is shown in Fig. 11. The temperature $T_{0s}(t)$ measured directly by the thermocouple is also shown for comparison.

The maximum gas temperature near the cone surface at $x = 19$ mm from the tip, during the plasma pulse, is calculated to be $T_{0p}^{\max}|_{\text{plasmaon}} = 610$ K. However, this high-temperature region is confined in a thin layer at the surface. This is evidenced by the outward decrease of the afterglow radiation intensity in the boundary layer.[19] This radiation intensity is function of the local temperature via the recombination rate of plasma. This assessment is also consistent with the measurement of the shock wave angle shown in Fig. 6b, in which no significant change of the shock angle during the plasma pulse can be observed in the conical surface region.

Summary

A plasma aerospike, formed by generating conical plasma around a slender physical spike for improving the aerodynamics of a blunt body in a supersonic flow, was investigated experimentally.

The experiments were performed in a Mach 2.5 nonionized airflow using a truncated 60-deg angle cone–cylinder model, with an axially attached isolated spike/electrode. The discharge power and energy, as well as the flow pressure and temperature on the surface of the model, were monitored. Shadow, schlieren, and plasma glow imaging techniques were simultaneously used for flow visualization.

The electrical discharge pulse, with a rise time of less than 1 ms and a slow decay of less than 50 ms, had a peak power of about 45 kW, and a total energy of about 150 J. Both the breakdown voltage and the peak discharge current decreased to about one-half of the corresponding values measured in stagnant air. The voltage to sustain the discharge decreased approximately by a factor of 2.5.

In the case of using a specific ratio of the spike length to model frontal diameter, $l/D = 0.81$, the discharge produced conically shaped plasma, which distributed symmetrically around the spike. A favorable aerodynamic change from a complicated structure of two interacting shocks, containing a tip-attached spike shock and a blunt-body bow shock, to a simple structure of a single tip-attached conical shock was observed. Such a change is equivalent to a modification of the body shape from a blunt body with slender attached spike to a 60-deg conical body, that is, a 70% increase in the body aspect ratio from $L/D_b = 0.5$ to $L_e/D_b = 0.85$, where L_e ($=1.7L$) is the height of this equivalent conical body.

As the plasma pulse modified the shock wave, the total pressure decrease at the frontal location of the model was more than 30% of, and the pressure increase on the cone surface was less than 5% of, the unperturbed pressure at the corresponding location. The pressure on the cylinder surface remained unchanged within the measurement errors. The pressure pulses in Figs. 8 and 9 have a pulse length of about 120 ms, which is longer than the pulse length of about 40 ms of the corresponding discharge power pulses shown in Fig. 7. In other words, the results indicate that the plasma affected the shock structure longer than did the electrical discharge pulse length.

The gas temperature on the cone surface increased up to about 2.5 times the unperturbed value during the discharge. However, this temperature increase, as the result of heating by the plasma, was confined in a thin layer near the surface, as indicated by the plasma afterglow intensity distribution.

In the cases of using spikes with much smaller aspect ratio, for example, $l/D = 0.27$, the discharge did not cause any noticeable modification of the shock wave pattern. It was also found in experiments that when the electrode/spike was used as the anode, the discharge did not introduce any significant influence on the shock wave pattern around the frontal part of the model. Note that all of these unfavorable cases were performed with the similar discharge pulse length and at about the same discharge energy as those in the favorable case, except that the discharges were not able to produce plasmas ahead of the bow shock generated by the blunt body. Therefore, the gas heating induced by the plasma pulse could not be the main cause of the observed shock wave modifications. Also note that the effect of gas heating is to reduce the local Mach number of the flow; as a consequence, the shock angle should increase, rather than decrease, as shown in Fig. 6.

The reported experiments have shown that the performance of a slender physical spike on the blunt-body aerodynamics can be greatly improved or controlled by generating conical plasma around it to form a plasma aerospike.

Acknowledgments

This work was supported by the U.S. Air Force Office of Scientific Research (AFOSR), Grants AFOSR-F49620-01-1-0392 and AFOSR-FA9550-04-1-0352. We thank Skip Williams, U.S. Air Force Research Laboratory at Hanscom Air Force Base, Massachusetts, for useful discussions and for his interest and valuable comments on the manuscript. We also thank Iraj Kalkhoran for useful suggestions and Lester Orlick for machining the model and for his assistance in running the wind tunnel.

References

[1]Ferri, A., "Supersonic Profiles," *Elements of Aerodynamics of Supersonic Flow*, Macmillan, New York, 1949, pp. 117–160.

[2]Ferri, A., and Clarke, J. H., "On the Use of Interfering Flow Fields for the Reduction of Drag at Supersonic Speeds," *Journal of the Aeronautical Sciences*, Vol. 24, No. 1, 1957, pp. 1–18.

[3]Chang, P. K., "Leading-Edge Flow Separation," *Separation of Flow*, 1st ed., Pergamon, Oxford, 1970, pp. 452–530.

[4]Resler, E. L., Jr., and Sears, W. R., "The Prospects for Magneto-Aerodynamics," *Journal of the Aeronautical Sciences*, Vol. 25, No. 4, 1958, pp. 235–245.

[5]Kantrowitz, A., *Flight Magnetohydrodynamics*, edited by F. H. Clauser, Addison Wesley Longman, 1960, pp. 221–232.

[6]Ziemer, R. W., "Experimental Investigation in Magneto-Aerodynamics," *ARS Journal*, Vol. 29, No. 9, 1959, pp. 642–647.

[7]Roth, J. R., and Sherman, D. M., and Wilkinson, S. P., "Applications of Plasma Aerodynamics: I—Boundary Layer Flow Control with a One Atmosphere Uniform Glow Discharge Surface Plasma," AIAA Paper 98-0328, Jan. 1998.

[8]Hill, G. A., "Ionized Boundary Layer Fluid Pumping System," U.S. Patent 3,095,163, filed 13 Oct. 1959; patented 25 June 1963.

[9]Katzen, E. D., and Kaattari, G. E., "Inviscid Hypersonic Flow Around Blunt Bodies," *AIAA Journal*, Vol. 3, No. 7, 1965, pp. 1230–1237.

[10]Gordeev, V. P., Krasilnicov, A. V., Lagutin, V. I., and Otmenicov, V. N., "Experimental Study of the Possibility of Reducing Drag by Employing Plasma Technology," *Fluid Dynamics*, Vol. 31, No. 2, 1996, pp. 313–317.

[11]Myrabo, L. N., and Raizer, Yu. P., "Laser Induced Air-Spike for Advanced Trans-Atmospheric Vehicles," AIAA Paper 94-2451, June 1994.

[12]Minucci, M. A. S., Toro, P. G. P., Oliveira, A. C., Ramos, A. G., Chanes, J. B., Pereira, A. L., Nagamatsu, H. T., and Myrabo, L. N., "Laser-Supported Directed-Energy 'Air Spike' in Hypersonic Flow," *Journal of Spacecraft and Rockets*, Vol. 42, No. 1, 2005, pp. 51–57.

[13]Exton, R. J., Balla, R. J., Shirinzadeh, G. J., Brauckmann, G. J., and Herring, G. C., "On-Board Projection of a Microwave Plasma Upstream of a Mach 6 Bow Shock," *Physics of Plasmas*, Vol. 8, No. 11, 2001, pp. 5013–5017.

[14]Levin, V. A., and Taranteva, L. V., "Supersonic Flow over Cone with Heat Release in the Neighborhood of the Apex," *Fluid Dynamics*, Vol. 28, No. 2, 1993, pp. 244–247.

[15]Riggins, D., Nelson, H. F., and Johnson, E., "Blunt-Body Wave Drag Reduction Using Focused Energy Deposition," *AIAA Journal*, Vol. 37, No. 4, 1999, pp. 460–471.

[16]Kuo, S. P., Kalkhoran, I. M., Bivolaru, D., and Orlick, L., "Observation of Shock Wave Elimination by a Plasma in a Mach 2.5 Flow," *Physics of Plasmas*, Vol. 7, No. 5, 2000, pp. 1345–1348.

[17]Kuo, S. P., and Bivolaru, D., "Plasma Effect on Shock Waves in a Supersonic Flow," *Physics of Plasmas*, Vol. 8, No. 7, 2001, pp. 3258–3264.

[18]Bivolaru, D., and Kuo, S. P., "Observation of Supersonic Shock Wave Mitigation by a Plasma Aero-Spike," *Physics of Plasmas*, Vol. 9, No. 2, 2002, pp. 721–723.

[19]Bivolaru, D., "On the Use of Plasma for Shock Wave Mitigation," Ph.D. Dissertation, Dept. of Mechanical, Aerospace, and Manufacturing Engineering, Polytechnic Univ., Brooklyn, NY, June 2002.

M. Auweter-Kurtz
Associate Editor